Research Article **www.ijcps.com**

International Journal of Chemical and Pharmaceutical Sciences
2017, Sep., Vol. 8 (2)

ISSN: 0976-9390
IJCPS

Spectroscopic, electrochemical and molecular docking studies on the biosensing of ofloxacin, Norfloxacin with different biomolecules

Rajendiran N* and Suresh M.

Department of Chemistry, Annamalai University, Annamalainagar, Tamilnadu, India

***Corresponding Author:** E-Mail**:** drrajendiran@rediffmail.com

Received: 20th Sep 2017, Revised and Accepted: 25th Sep 2017

ABSTRACT

Biosensing property of ofloxacin and norfloxacin with different biomolecules (DNA, RNA and BSA) are investigated by UV–Visible absorption spectroscopy, fluorescence spectroscopy, cyclic voltammetry and molecular docking methods. Upon increasing the concentration of the biomolecules, the absorption maxima of ofloxacin and norfloxacin are red shifted in aqueous solutions whereas red or blue shifted in the fluorescence spectra. The negative free energy changes suggest that the interaction processes are spontaneous. The binding constant (K_a) of the drugs with biomolecules were calculated by Benesi-Hildebrand equation. Cyclic voltammetry results suggested that when the drug concentration is increased, the anodic electrode potential increased. To find the most favourable structure, the geometry of complex was investigated by molecular docking method. The results showed that hydrophobic forces, electrostatic interactions, and hydrogen bonds played vital roles in the drugs with biomolecules binding interaction. The results of molecular docking calculation clarify the binding mode and the binding sites which are in good accordance with the experiment results.

Keywords: Ofloxacin, Norfloxacin, DNA, RNA, BSA, Biosense.

1. INTRODUCTION

The binding of DNA to a neutral curved surface can be enhanced by different kinds of forces and processes, including hydrogen bonding, van der Waals and hydrophobic interactions, and the release of counter ions and solvent from DNA or the particle substrate [1].Such binding is favored, in terms of energetic cost, if the DNA is already bent, so that it can match the curved surface [2]. Because of its negatively charged phosphate backbone, double-stranded DNA can easily interact with positively charged particles or particles having acidic hydrogens on their surfaces.

The functional and structural diversities of RNA provide numerous opportunities for academic researchers and pharmaceutical industry to develop small molecules to target specific RNA for treating a variety of diseases, such as bacteria or virus infections [3]. The RNA secondary structure of base pairing is more conservative than its primary sequence, so the potential for slower development of drug resistance against small molecules is one of the advantages of targeting RNA over traditional protein targets. Aminoglycosides, a class of structurally diverse aminocyclitols with potent antibiotic and antiviral activities are intensively and well-studied RNA binders [4].

Serum albumins are major transport proteins found in plasma and have been extensively studied for years [5–9]. Bovine serum albumin (BSA) has 583 amino acid residues arranged in a single polypeptide chain and 17 disulphide bridges leading to a series of nine loops. This gives the protein a roughly heart-shaped structure. The protein has three domains I, II and III each with two subdomains IA, IB, IIA, IIB, IIIA and IIIB. BSA has two tryptophan residues Trp-134 and Trp-212. While Trp-212 is more exposed, Trp-134 resides deep inside a hydrophobic pocket. Serum albumins have served as model proteins for a large variety of bio-chemical and bio-physical studies and continue to garner interest owing to their easy handling, drug-binding capacities and other standard model properties. Surfactants bind strongly to proteins leading to major conformational changes in the protein and these surfactant induced uncoiling of proteins are widely studied owing to the

structural information that can amassed from them. Interactions of the model protein BSA with various cationic, anionic and neutral surfactants have been reported and a multitude of models proposed to explain some of these binding processes [10–15]. The binding isotherms for these surfactants-protein systems were constructed from the various studies carried out and show distinct regions of binding.

Fluoroquinolones (FQs) drugs inhibit the topoisomerase enzymes activity which involved in bacterial DNA synthesis. OFLX is a member of FQs drug family and active against both Gram-positive and Gram-negative bacteria by inhibiting DNA gyrase.

Ofloxacin((7)-9-fluoro-2,3-dihydro-3-methyl-10-(4-methyl-1- piperazinyl)-7-oxo-7H-pyrido[1,2,3-de]-1,4-benzoxacine-6-carboxilic acid) isanalidixic acid analog with broad spectrum antibacterial activity [Figure.1]. It belongs to the fluorquinolones group, which act as specific inhibitors of the bacterial DNA-gyrase, the enzyme responsible for converting double-stranded DNA into a negative super- helical form [16].

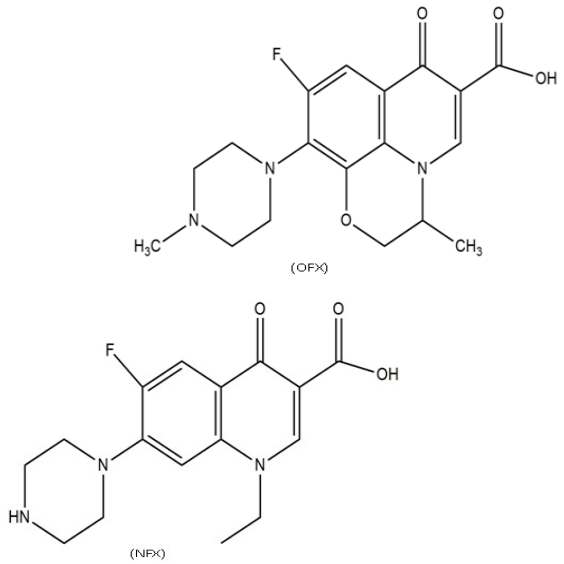

Figure – 1: Chemical structure of ofloxacin (OFX), and norfloxacin (NFX).

Norfloxacin (1-ethyl-fluoro-1,4-dihydro-4-oxo-7-(1-piperazinyl)-3-quinolinecarboxylic acid) (NFX) [Figure 1] belongs to the group of fluoroquinolones, and is a synthetic, broadspectrum antibacterial agent that exhibits high antimicrobial activity in vitro against a wide variety of Gram-negative and Gram-positive bacteria, including gentamicin resistant Pseudomonas aeruginosa and b-lactamase positive Neisseria gonorrhoeae [17]. NFX is used to treat a variety of bacterial infections in many third world countries. Excellent therapeutic effects have been shown in the treatment of respiratory, biliary and urinary tract infections, especially those caused by Gram-negative rather than Gram-positive disorders

2. EXPERIMENTAL

2.1. Materials

OFX, NFX DNA, RNA and BSA were purchased from Sigma-Aldrich Chemical Company, USA, and used without further purification. Triply distilled water was used for the preparation of aqueous solutions.

2.2. Methods

The concentration of stock solution of the drugs (OFX and NFX) was 2×10^{-3} M. The stock solution (0.2 ml) was transferred into 10 ml volumetric flasks. The solution was diluted to 10 ml with triply distilled water and shaken thoroughly. To this, varying concentrations of the drug solution (2×10^{-3} to 2×10^{-5} M) were added. The final concentration of OFX and NFX drugs in all the flasks was 2×10^{-5} M. Biomolecules solutions were prepared in 1×10^{-6} M. The different volume of solution (0.1, 0.3, 0.5, 0.7, 0.9, 1.0 ml) added to above mentioned 10 ml flask. The experiments were carried out at room temperature. All solutions were stored in a refrigerator at 4 °C.

2.3. Instruments

Absorption spectral measurements were carried out with a UV–visible spectrophotometer (model-UV-2600, Shimadzu, Japan) and fluorescence measurements were performed on a spectrofluorophotometer (model- RF-5301PC, Shimadzu, Japan) equipped with 1.0 cm quartz cells. Cyclic voltammetry measurements were performed through an electrochemicalwork station (model-CHI 620D, CH Instruments, USA) with a three electrode system: surface area 0.1963 cm^2 glassy carbon electrode asworking electrode, saturated silver electrode as reference electrode and a platinum foil as counter electrode. Prior to use, the working electrode was polished with 0.05 μm alumina and thoroughly washed in an ultrasonic bath for 5 min. Before experiments, the solution within a single compartment cell was deaerated by purging with pure N_2 gas for 5 min.

2.4. AutoDock

AutoDock is a software suite for performing automated docking by simulated annealing, local gradient searches and genetic algorithms [18-20]. The combination of a genetic algorithm with inheritance of local optimizations, yielding a Lamarckian genetic algorithm, endows autodock with very good search performance. In addition to an efficient search algorithm, recent versions of autodock include a ΔG bind correlation

derived from molecular conformations. As of version 4.2.6, autodock for Linux, Mac OS X and Windows is available under the GNU General Public License (GPL) and can be downloaded free of charge from http:// autodock.scripps.edu. At the time of writing, two versions of autodock, autodock 4.2.6 and autodock vina, are available. It should be noted that while the techniques presented in this chapter may be adaptable to autodock vina, these techniques are presented with autodock 4.2.6 in mind. Furthermore, scoring functions from autodock versions 1 to 3 may be adapted for use in either autodock 4.2.6 or autodock vina. To successfully prepare carbohydrate models for use in autodock, several related pieces of software will be useful. If desired, nearly all of the protein and drug preparation can be done using the autodock tools (ADT) available from the same website as autodock. However, the reader may wish to provide his her own tools for molecule preparation as appropriate. Gasteiger partial charges were added to the drug atoms. Non-polar hydrogen atoms were merged, rotatable bonds were defined and the docking calculations were carried out on 1bna (dna), 2ke6 (rna), 3v03 (bsa), protein model. Hydrogen atoms, solvation parameters and kollman united atom type charges were added with the aid of autodock tools [21]. Affinity (grid) maps of 0.375 Å spacing and 20×20×20 Å grid points were generated using the auto grid program [19]. Autodock parameter set- and distance-dependent dielectric functions were used in the calculation of the van der waals and the electrostatic terms, respectively. Docking simulations were performed using the lamarckian genetic algorithm (LGA) and the solis & wets local search method. Initial position, orientation, and torsions of the drug molecules were set randomly. Each docking experiment was derived from 10 different runs that were set to terminate after a maximum of 25 x10^4 energy evaluations. The population size was set to 150. During the search, a translational step of 0.2 Å, and quaternion and torsion steps of 5 were applied [22-27].

3. Results and discussion

3.1. Absorption Spectral Study

[Tables 1, 2] and [Figures 2, 3] depict the absorption spectra of OFX and NFX in aqueous solution containing different concentrations of DNA, RNA and BSA. In water, OFX absorption maxima appears at 331, 288, 256 and 248 nm and NFX absorption maxima appears at 332, 322, 273 and 225 nm. The absorption spectra of OFX and NFX can be divided into three regions: (i) the longer wavelength (LW) absorption bands comprising the region at ~331 nm for OFX and 332 nm for NFX, (ii) the middle wavelength (MW) band is around 288 nm for OFX and 322 nm for NFX, and (iii) the shorter wavelength (SW) absorption band is at 256 nm for OFX and 273 nm for NFX is shown in [Figures. 2 and 3].

In aqueous DNA, RNA and BSA solution, the absorption bands are observed at ~258, ~257 and ~278 nm respectively. With increasing the concentration of biomolecules, the absorption intensities of DNA RNA and BSA were completely lost whereas OFX in DNA and BSA, absorption intensities were decreased. However in RNA, absorption intensities were increased. In NFX solution, upon increasing the concentration of the DNA and RNA, the absorption intensities were, whereas in BSA the absorption intensities were increased in longer wavelength and decreased in both middle and Shorter wavelength.

The summarized results of the sensing of the drugs with the biomolecules are given below: i) with increasing the DNA concentration, the absorbance of both OFX and NFX are decreased, (ii) upon increasing the concentration of RNA, the absorbance of OFX is increased where as NFX is decreased (iii) increasing the concentration of BSA the absorbance of OFX is decreased where as NFX is take both decreased and increased, (iv) in OFX with on increasing the concentration of the DNA and BSA, the absorption maxima red shifted from 331 nm to 337 nm, while in RNA, it is blue shifted from 331 nm to 326 nm. (v) in NFX with on increasing the concentration of the DNA and RNA, the absorption maxima red shifted from 332 nm to 338 nm, while in BSA, there is no spectral changes. The above results indicate that biomolecules are interacted with OFX and NFX drugs. The insert Figs. 2 and 3 depict the changes in the absorption and fluorescence intensities with the drug concentrations indicating that biomolecules could bind with the OFX and NFX drugs. When compared to biomolecules, the decrease in absorbance is more in NFX-DNA than that of drug with biomolecule interactions.

In general, several driving forces have been postulated for the interaction of drug with DNA or BSA compounds [18]. Four main types of non-covalent interactions occur in drug-protein binding: (i) hydrogen bonds, (ii) van der Waals interactions, (iii) electrostatic Upon increasing

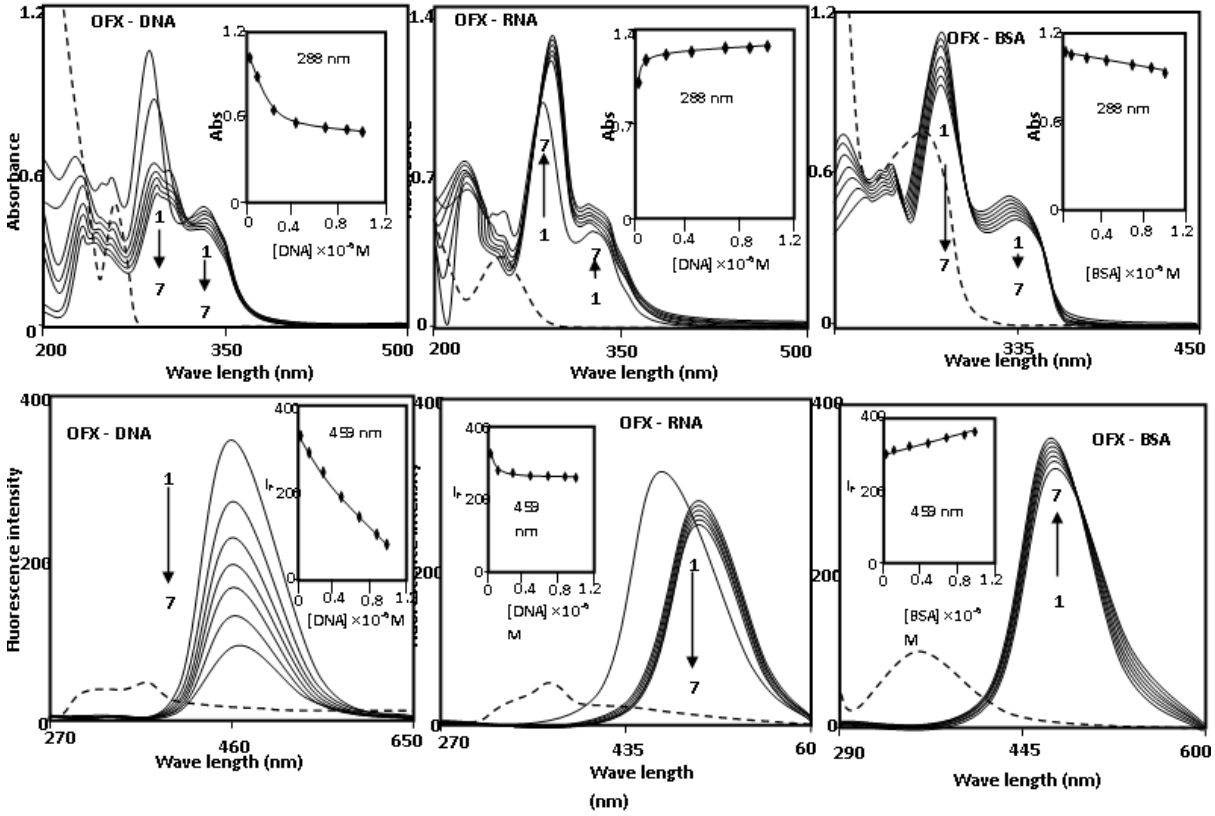

Figure – 2: Absorbance and fluorescence spectra of drugs (OFX) with different concentrations of Biomolecules (M x 10^{-6}): 1) 0, 2) 1, 3) 3, 4) 5, 5) 7 and 6) 9, 7) 10; dotted lines: DNA or RNA or BSA Inset fig: Absorbance and fluorescence intensity vs. Biomolecules concentration. (Ref: DNA or RNA or BSA).

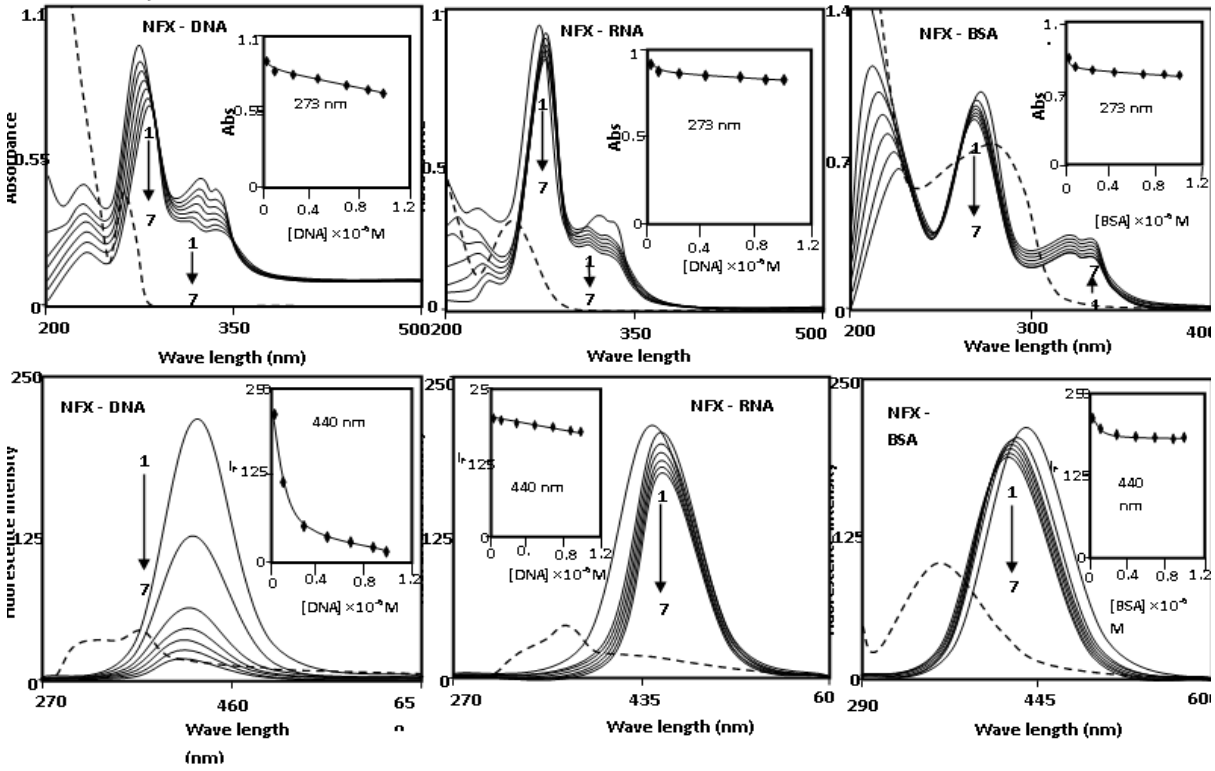

Figure - 3: Absorbance and fluorescence spectra of drugs (NFX) with different concentrations of Biomolecules (M x 10^{-6}): 1) 0, 2) 1, 3) 3, 4) 5, 5) 7 and 6) 9, 7) 10; dotted lines: DNA or RNA or BSA Inset fig: Absorbance and fluorescence intensity vs. Biomolecules concentration. (Ref: DNA or RNA or BSA).

Table – 1: Absorption and fluorescence maxima of OFX (2 x 10^{-4} M) with different DNA, RNA and BSA concentrations.

Concentration of Biomolecules (M)	DNA			RNA			BSA		
	OFX			OFX			OFX		
	λ_{abs}	log ε	λ_{flu}	λ_{abs}	log ε	λ_{flu}	λ_{abs}	log ε	λ_{flu}
Proteins only	258	5.68	364	257	5.56	363	278	5.86	340
OFX only	331	4.11		331	4.05		331	4.14	
	288	4.42	459	288	4.41	459	288	4.46	459
	256	4.15		256	4.12		256	4.19	
	248	4.14		248	4.11		248	4.18	
0.1	332	4.10		326	4.09		332	4.14	
	289	4.34	461	291	4.50	494	288	4.45	458
	257	4.06		259	4.01		257	4.18	
	248	4.09		247	4.08		249	4.17	
0.3	333	4.09		326	4.09		333	4.13	
	290	4.17	465	291	4.50	495	288	4.44	457
	258	4.04		259	4.00		258	4.17	
	249	4.07		247	4.07		250	4.16	
0.5	334	4.08		326	4.11		334	4.12	
	291	4.15	468	291	4.50	496	288	4.43	456
	259	4.02		259	3.99		259	4.17	
	250	4.05		247	4.06		251	4.15	
0.7	335	4.07		326	4.11		335	4.11	
	292	4.14	471	291	4.51	497	288	4.42	455
	260	4.00		259	3.98		260	4.16	
	251	4.03		247	4.05		252	4.15	
0.9	336	4.06		326	4.12		336	4.10	
	293	4.12	476	291	4.51	498	288	4.41	454
	261	3.97		259	3.96		261	4.15	
	252	4.02		247	4.05		253	1.14	
1	337	4.05		326	4.13		337	4.10	
	294	4.11	479	291	4.52	499	288	4.40	453
	262	3.96		259	3.96		262	4.15	
	253	4.01		247	4.03		253	4.13	
Excitation wavelength (nm)			340			340			340
K (1:1) x10^5 M^{-1}	3.6		5.0	7.0		7.8	2.1		2.3
ΔG (kcalmol^{-1})	-7.61		-7.78	-8.07		-8.12	-7.34		-7.40

Table - 2: Absorption and fluorescence maxima of NFX (2 x 10^{-4} M) with different concentrations of DNA, RNA and BSA

Concentration of Biomolecules (M)	DNA			RNA			BSA		
	NFX			NFX			NFX		
	λ_{abs}	log ε	λ_{flu}	λ_{abs}	log ε	λ_{flu}	λ_{abs}	log ε	λ_{flu}
Proteins only	258	5.68	364	257	5.56	363	278	5.86	340
NFX only	322	4.06	440	322	3.90	440	322	3.72	440
	332	4.10		332	3.92		332	3.76	
	273	4.40		273	4.38		273	4.04	
	225	4.07		225	4.04				
0.1	321	4.03	437	316	3.84	446	322	3.70	435
	333	4.08		329	3.87		332	3.75	
	274	4.37		276	4.38		270	4.02	
	226	4.01		227	4.01				
0.3	320	4.01	435	316	3.83	447	322	3.69	430
	334	4.05		329	3.85		332	3.73	
	275	4.36		276	4.37		270	3.55	
	227	3.96		228	3.97				
0.5	319	3.99	434	315	3.81	447	322	3.67	425
	335	4.02		329	3.83		332	3.71	
	276	4.34		276	4.37		270	4.00	
	228	3.94		229	3.92				
0.7	318	3.97	433	315	3.79	447	322	3.63	423
	336	3.99		329	3.81		332	3.68	
	277	4.32		276	4.37		270	3.99	
	229	3.89		230	3.86				
0.9	317	3.94	432	314	3.78	447	322	3.62	420
	337	3.96		329	3.81		332	3.66	
	278	4.32		276	4.36		270	3.98	
	230	3.85		231	3.79				
1	316	3.92	431	314	3.75	447	322	3.59	418
	338	3.94		329	3.78		332	3.63	
	279	4.29		276	4.36		270	3.96	
	231	3.80		232	3.66				
Excitation wavelength (nm)			320			320			320
K (1:1) x10^5 M^{-1}	2.0		7.3	3.3		5.1	3.4		6.5
ΔG (kcalmol^{-1})	-8.07		-8.66	-7.56		-7.89	-7.52		-8.05

Table - 3: CV for OFX with Biomolecule (scan rate, 100 mV $s^{-1,}$ concentration of OFX ~ 2 × 10^{-4} M; Biomolecule concentration ~ M × 10^{-6}.

Drug-DNA	Drugs concentration (× 10^{-6})	E_{pa} (mV)	I_{pa} (µA	E_{pc} (mV)	I_{pc} (µA	E_{pa}-E_{pc}/2	I_{pa}/I_{pc}
DNA only	2× 10^{-6}	-573	-8.405	-228	11.09	-172	-0.7578
		273	-3.264	602	10.38	-164	-0.3144
RNA only	2× 10^{-6}	-400	-5.809	-296	10.14	-52	-0.5728
		069	-6.873	508	9.16	-219	-0.7503
BSA only	2× 10^{-6}	-406	-12.38	-379	48.38	-13	-0.2588
		205	-9.600	263	54.96	-29	-0.1746
OFX only	2	-1183	-4.011			-497	
		028	0.553	-189	1.628	14	-2.4637
		1092	2.625			546	
OFX-DNA	2	-365	-3.767	-154	22.56	-105	-0.0669
		258	5.326	589	13.19	-165	0.4037
	4	-371	-4.541	-154	24.31	-108	-0.1868
		258	5.672	561	14.33	-151	0.3958
	8	-389	-5.433	-154	26.47	-117	-0.2052
		258	5.981	547	15.98	-144	0.3742
	10	-395	-5.942	-154	28.65	-120	-0.2074
		258	6.230	531	17.05	-136	0.3653
OFX-RNA	2	-792	-11.63	-370	13.84	-211	-0.8403
		261	-7.523	218	12.76	21	-0.5895
	4	-754	-12.94	-359	15.80	-197	-0.8189
		261	-7.615	230	13.13	15	-0.5799
	8	-687	-13.88	-337	17.60	-175	-0.7886
		261	-7.734	258	15.19	1	-0.5091
	10	-640	-14.20	-321	18.96	-159	-0.7514
		261	-7.815	281	16.98	-10	-0.4601
OFX-BSA	2	-783	-9.824	-5	9.568	-389	-0.7821
	4	-792	-7.261	-8	8.857	-392	-0.8198
	8	-851	-6.021	-12	7.143	-419	-0.8429
	10	-890	-5.630	-18	6.361	-436	-0.8852

towards BSA (v) when compared to RNA and BSA, the absorption and emission intensities changes in NFX in DNA is higher than that of RNA and BSA.

Utilizing emission or absorption changes of norfloxacin in the presence of DNA, a Benesi-Hildebrand type plot can be constructed. By plotting the reciprocal absorbance at a fixed wavelength vs. reciprocal concentration of DNA, the equilibrium constant for formation of the norfloxacin-DNA complex can be estimated from the ratio of the slope to the intercept

The observed spectral changes and the shift in the position of λ_{max} of OFX and NFX are likely to reflect direct or indirect interactions of these biomolecules with the hydrophobic and hydrophilic regions. The above changes reflect not only the formation of 1:1 complex between the drugs and the biomolecules, but also indicate that the binding site of the drug is hydrophobic in

Table - 4: CV for NFX with Biomoleccule (scan rate, 100 mV $s^{-1,}$ concentration of drugs ~ 2 × 10^{-4} M; Biomolecule concentration ~ M × 10^{-6}.

Drug-DNA	Drugs concentration (× 10^{-6})	E_{pa} (mV)	I_{pa} (µA	E_{pc} (mV)	I_{pc} (µA	E_{pa}-E_{pc}/2	I_{pa}/I_{pc}
DNA only	2× 10^{-6}	-573	-8.405	-228	11.09	-172	-0.7578
		273	-3.264	602	10.38	-164	-0.3144
RNA only	2× 10^{-6}	-400	-5.809	-296	10.14	-52	-0.5728
		069	-6.873	508	9.16	-219	-0.7503
BSA only	2× 10^{-6}	-406	-12.38	-379	48.38	-13	-0.2588
		205	-9.600	263	54.96	-29	-0.1746
NFX only	2	-495	-5.411	-239	11.15	-128	-0.4852
		179	-6.019	320	10.18	-70	-0.5912
				733	11.30	-366	
NFX-DNA	2	-563	-7.673	-395	14.13	-84	-0.5430
		282	-6.217	406	13.55	-62	-0.4588
	4	-559	-7.414	-361	15.85	-99	-0.4677
		261	-6.679	428	14.80	-83	-0.4512
	8	-541	-7.139	-332	16.71	-104	-0.4272
		243	-6.921	441	15.61	-99	-0.4433
	10	-529	-6.902	-299	17.64	-115	-0.3912
		222	-7.140	467	16.38	-122	-0.4359
NFX-RNA	2	-663	-7.319	-366	5.832	-148	-1.2549
		100	-4.881			50	
	4	-697	-6.146	-381	4.671	-158	-1.3157
		136	-4.936			68	
	8	-741	-5.623	-408	3.691	-166	-1.5234
		167	-5.023			83	
	10	-783	-4.952	-432	2.124	-175	-2.3314
		206	-5.136			103	
NFX-BSA	2	-510	-4.952	-221	10.70	-144	-0.4628
		235	-9.600			117	
	4	-571	-3.698	-218	9.991	-176	-0.3701
		260	-4.771			130	
	8	-630	-2.859	-212	9.231	-209	-0.3097
		282	-3.180			141	
	10	-698	-1.331	-209	8.879	-244	-0.1499
		299	-2.065			149	

the concentration of biomolecules, the emission intensities of DNA, RNA and BSA were completely lost whereas in OFX and NFX the emission intensities are increased or decreased. The results of the sensing of the drugs with the biomolecules are given below:

(i) In the excited state, upon increasing the DNA concentration the emission intensity of OFX is decreased and the spectral maximum is red shifted from 459 nm to 479 nm, (ii) in RNA, the fluorescence intensity of OFX is decreased and the maximum is red shifted from 459 nm to 499 nm, (iii) Interestingly in BSA, the emission intensity is increased and the emission maximum is blue shifted from 459 nm to 453 nm.

In NFX (i) with increasing the DNA, RNA and BSA concentrations, emission intensity is decreased, (ii) the spectral maximum is blue shifted from 440 nm to 431 nm towards DNA (iii) the spectral maximum is red shifted from 440 nm to 447 nm towards RNA, (iv) the spectral maximum is blue shifted from 440 nm to 418 nm

interactions, and (iv) hydrophobic forces [20].These results suggest that there is one binding site in DNA, RNA and BSA for OFX and NFX during their interaction which is further confirmed by a modified Benesi, and Hildebrand equation [28].

Incremental addition of DNA to the aqueous buffer solution of drug results in a progressive change in absorbance for OFX species and NFX species. The difference is initially higher and further additions gradually decrease the absorbance. Compared to NFX less change observed in OFX. On the basis of result it can be argued that the sensing property of NFX is higher than of OFX in DNA interaction. The changes in the absorption spectra suggest that the drug sense the biomolecules.

Electronic absorption spectroscopy is an effective method to examine the binding mode of OFX, NFX with biomolecules [29]. The mutual effect of the drugs with biomolecules has been studied with UV spectroscopy in order to investigate the possible binding modes to drug with biomolecule and to calculate the binding constants to drug (Kb). In UV experiments, the spectra of drug in the presence of each concentration have been recorded for a constant drug concentration. Drug concentration were 1 × 10−4 M to 1 × 10−5 M in the absence and presence of biomolecules. It has been reported that biomolecules can provide several distinctive binding sites for all drugs; namely, groove binding, electrostatic binding to phosphate group, and intercalation [29, 30, 31, 32].

The binding constant of both the drug:biomolecules complexes are calculated by the Benesi–Hildebrand equation. The values of the binding constant (K) for OFX-DNA, OFX-rna and OFX-bsa were obtained from the absorption at 331 nm and NFX-DNA, NFX-rna and NFX-bsa were obtained from the absorption at 332 nm according to the methods published in the literature [33] For weak binding affinities, the data were, treated using linear reciprocal plots based on equation (1) [34]

$$1/(A-A_0) = 1/(A_\infty-A_0) + 1/K(A_\infty-A_0) \times 1/ [\text{Biomolecules}] \quad (1)$$

Where A_0 is absorbance of OFX at 331 nm in the absence of biomolecules, A∞ is final absorbance of the drug-DNA and A is the absorbance recorded at different biomolecules concentrations. The double reciprocal plot of $1/(A–A_0)$ versus 1/ [biomolecules] is linear and the best binding constant (K) can be estimated from the ratio of the intercept to the slope [29].

3.2. Fluorescence emission spectrometry

[Tables 1, 2] and [Figures 2, 3] shows the fluorescence spectra of OFX and NFX in aqueous solution as a function of DNA, RNA and BSA concentration. The fluorescence characteristics of OFX and NFX in aqueous solutions are seen to undergo drastic changes in the presence of DNA, RNA and BSA. These will be partially due to conformational changes of the drugs. The emission maximum of DNA, RNA and BSA are noticed at ~364, ~363 and ~340 nm respectively. The emission spectrum of OFX and NFX In aqueous solution, the emission maxima of OFX and NFX appear at 459 nm and 440 nm respectively.

Table - 5: Result of drug receptor interaction

Proteins	Drugs	Binding energy ΔGb (kcal/mol)	Intermolec. Energy kcal/mol	Torsional energy	Total Internal energy	Inhibition constant (uM)	vdW + H bond + desolv Energy kcal/mol	Electro static Energy kcal/mol	Ligand efficiency	Unbond energy	refRMS
OFX	DNA	-6.30	-7.19	0.89	-0.84	24.15	-5.28	-1.92	-0.24	-0.84	30.45
	RNA	-5.38	-6.27	0.89	-0.83	114.06	-5.96	-0.32	-0.21	-0.83	29.84
	BSA	-5.97	-6.87	0.89	-0.85	41.82	-5.09	-1.78	-0.23	-0.85	106.60
NFX	DNA	-7.32	-8.51	1.19	-0.03	4.34	-6.33	-2.18	-0.32	0.03	25.89
	RNA	-4.90	-6.09	1.19	-0.56	257.66	-3.96	-2.13	-0.21	-0.56	28.00
	BSA	-5.54	-6.73	1.19	-0.64	86.8	-5.01	-1.73	-0.24	-0.64	101.45

Table - 6: List of interactions and its values of OFX withBiomolecules

OFX	DNA	OFX	RNA	OFX	BSA
OFX:O	DG14:H22	OFX:O	RNA	OFX:O	LYS533:HZ2
OFX:O	DG2:H21	OFX:O	A32:PHO2	OFX:O	GLN416:OE1
OFX:O	DG24:H21	OFX:O	A34:H3	OFX:O	THR419:HN
OFX:O	DG24:H3	OFX:O	A31:H3	OFX:O	LYS533:HZ2
OFX:O	DG10:H21	OFX:O	A32:H3	OFX:O	LYS439:HZ1
		OFX:O	U17:O2	OFX:O	LYS20:HZ1
		OFX:N	U16:O2P		

Table - 7: List of interactions and its values of NFX with Biomolecules

NFX	DNA	NFX	RNA	NFX	BSA
NFX:H	DA17:O3	NFX:H	U5:OP1	NFX:O	LYS499:HZ3
NFX:O	DG14:H22	NFX:O	G46:H3	NFX:O	LYS533:HZ2
NFX:H	DG4:OP1	NFX:O	G46:H22	NFX:O	TYR496:HH
NFX:O	DG24:H3	NFX:H	C35:OP2	NFX:O	HIS3:HN2
NFX:O	DG24:H21	NFX:O	G10:H7	NFX:O	ARG10:HH21
NFX:H	DG14:H3	NFX:H	U36:OP1	NFX:H	GLU293:OE1
NFX:H	DA17:OP1	NFX:O	C35:H3	NFX:O	LYS275:HZ2
NFX:O	DG12:H21	NFX:H	C35:H3	NFX:H	ASP172:OD2
NFX1:H	DC21:OP2	NFX:H	U17:O4P	NFX:H	GLU45:OE2
		NFX:H	A33:O2P	NFX:H	LYS64:HZ3
		NFX:H	U4:OP1	NFX:H	ILE297:HN
		NFX:O	G46:H3		
		NFX:O	G46:H22		
		NFX:H	A34:O4P		
		NFX:H	U15:O4P		

nature. The fluorescence spectrum shifts due to change in polarity of the environment; however the change in fluorescence intensity of the flexible molecules depends not on the polarity of the medium, but also on the constraint provided by the media. The binding constant values were estimated from the fluorescence emission data by using Benesi–Hildebrand equation (2) [28]

$$1/(I-I_0) = 1/(I_\infty-I_0) + 1/K(I_\infty-I_0) \times 1/[\text{Biomolecules}] \quad (2)$$

Where I_0 is the emission intensities in the absence of biomolecules, I and I_∞ are the emission intensities in the presence of biomolecules and when the drug is completely solubilized in biomolecules respectively. The emission intensities at 459 nm and 440 nm for OFX and NFX respectively used as for Benesi–Hildebrand plot of the drugs-biomolecule interactions [Figure 2]. The binding constant (*K*) is determined from the ratio of intercept and slope of Benesi–Hildebrand plot of the emission intensity. Using the value of K, the free energy change (ΔG kJ/mol^{-1}) for the drug–biomolecule complexation is determined and presented in [Tables 1, 2]. From the value of binding constant, it can be seen that drugs binds strongly to dna, rna and BSA and the nature of binding with NFX is stronger than OFX. Free energy change indicates spontaneity of complexation process for both cases. The values obtained for *K* and Δ*G* are well in agreement with that obtained for such complexation processes studied earlier [35,36]. The good linear correlations drug-biomolecule for$1/(I–I_0)$ versus 1/ [biomolecules] plot confirm the formation of 1:1 complex between the drug- biomolecules are given in [Figure 4]. The binding constants thus obtained are $5 \times 10^5\,M^{-1}$, $7.8 \times 10^5\,M^{-1}$, $2.3 \times 10^5\,M^{-1}$, and $7.3 \times 10^5\,M^{-1}$, $5.1 \times 10^5\,M^{-1}$, $6.5 \times 10^5\,M^{-1}$ for OFX-DNA, OFX-RNA, OFX-BSA and NFX-DNA, NFX-RNA, NFX-BSA respectively.

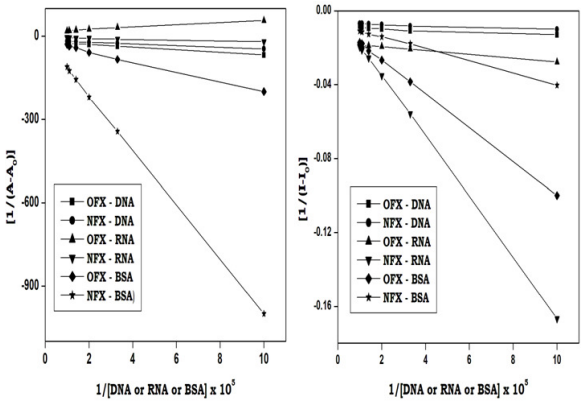

Figure - 4: Absorption spectra and Fluorescence spectra of Benesi-Hildebrand plot for the complexation of OFX and NFX with DNA, RNA, BSA (Plot of $1/A-A_0$ and $1/I-I_0$ vs 1/ [DNA (or) RNA (or) BSA]).

In general, several driving forces have been postulated for the interaction of guest with adenine and BSA compounds [37]. Four main types of non-covalent interactions occur in drug-protein binding: (i) hydrogen bonding, (ii) van der Waals interactions, (iii) electrostatic interactions, and (iv) hydrophobic forces [38]. Thermodynamic parameter (ΔG) of the binding reaction provides the evidence to confirm the binding force. Based on the free energy (ΔG) calculated for the interaction of these drugs, the hydrogen bonding interaction, van der Waals interaction and breaking of the water cluster around this polar drug compound mainly dominate the driving force for drug with adenine or BSA interaction. Thermodynamic parameters of the binding reaction provide the majority of the evidence to confirm the binding force. Hence, the free energy change (ΔG) can be derived from the equation:

$$\Delta G = - \ln K RT \qquad (3)$$

Where, K is the binding constant at a corresponding temperature; R is the gas constant; and T is the absolute temperature. Meanwhile, the negative value of ΔG indicated the spontaneity of the binding between sulfa drugs and BSA. Further, ΔG for BSA-drug is more negative than that of adenine – drug indicates the former binding is more spontaneous than later. The change in free energy for the drug-biomolecule complexations are −7.78, −8.12 , −7.40 and -8.66, -7.89, 8.05 kcal mol^{-1} for OFX-DNA, OFX-RNA, OFX-BSA and NFX-DNA, NFX-RNA, NFX-BSA respectively.

3.3. Cyclic voltammetry

In our studies, all complexes were subjected to a cyclic voltammetric study to characterize their electrochemical behavior on the glassy carbon electrode (GCE) compared to DNA. The supporting electrolyte has a significant effect on the electrooxidation/electroreduction of the complexes at the GCE. In order to substantiate the interaction of OFX and NFX drugs with DNA, RNA and BSA were measured in cyclic voltammetry (CV) method. The application of electrochemical methods to the study of drug intercalation to biomolecules provides a useful complement to the previously used methods of investigation, such as UV–visible spectroscopy and fluorescence spectroscopy. Multiple oxidation states of the same species as well as mixtures of several interacting species can be observed simultaneously [22-27]. Equilibrium constants (K) for the sensing of the drug-biomolecule complexes with biomolecules can be obtained from shifts in peak potentials, and the number of base pair sites involved in bindings through intercalative, electrostatic or hydrophobic interactions by the reliance of the current passed during oxidation or reduction of the bound species on the amount of biomolecules added. Cyclic voltammetry is widely used for the evaluation of mode of action and binding strength of drug–biomolecule interaction. This technique is predominantly useful for chemical compounds due to their accessible redox states. As in CV the scan is revered so the fate of the species in the backward scan can also be studied. The peak potential and peak current of the compound changes in the presence of biomolecules if the compound interacts with it are discussed. The variation in peak potential and peak current can be exploited for the determination of binding parameters.

[Tables 3, 4] and [Figures 5 to 8] show the cyclic voltammetry data of OFX and NFX drugs in absence and presence of DNA, RNA and BSA at glassy carbon electrode in Tris - HCl buffer (pH 7). [Tables 3, 4] and [Figures. 5 to 8] depicts the CV data and anodic and cathodic peaks of OFX and NFX with varying concentration of DNA, RNA and BSA. When OFX and NFX was added to the DNA, RNA and BSA solution, oxidation and reduction peaks shifted towards high and low potentials respectively and increase or decrease of oxidation current was observed.

The results in the [Tables 3, 4] of the sensing of the drugs with the biomolecules are given below:

In DNA, (i) the anodic peak potential (E_{pa}) and cathodic peak potential (E_{pc}) observed at -573, 273 mv and – 228, 602 mv respectively, (ii) the anodic peak current (I_{pa}) and cathodic peak current (I_{pa}) observed at -8.4, -3.3 mv and 11.0, 10.4 mv respectively. **In RNA**, (i) the anodic and cathodic peak potential observed at -400, 69 mv and – 296, 508 mv respectively, (ii) the anodic and cathodic peak current observed at -5.8, -6.9 mv and 10.1, 9.1 mv respectively. **In BSA**, (i) the anodic and cathodic peak potential observed at -

406, 205 mv and – 379, 263 mv respectively, (ii) the anodic and cathodic peak current observed at -12.4, -9.6 mv and 48.4, 54.9 mv respectively.

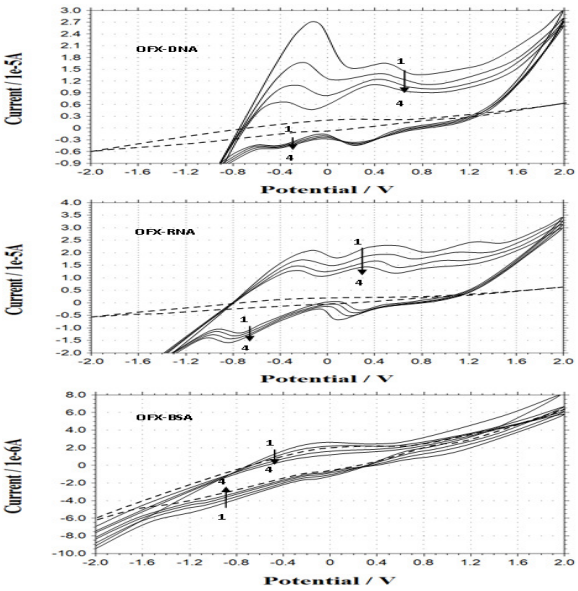

Figure - 5: Cyclic voltammograms of a OFX with additions of different concentration of Biomolecules (in platinum electrode; scan rate, 100 mV $s^{-1,}$ concentration of OFX - 2×10^{-4} M; Biomolecule concentration ($M\times10^{-6}$) – 0.2, 0.4,0.8, & 1.0).

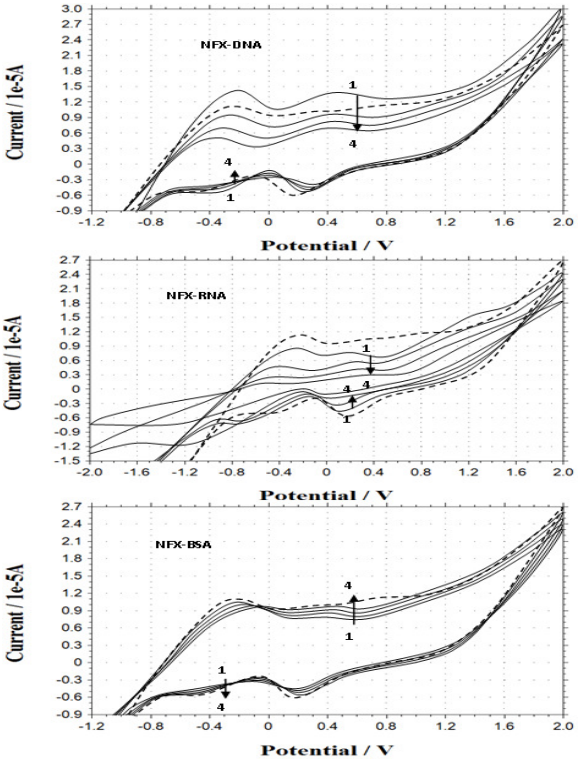

Figure – 6: Cyclic voltammograms of a NFX with additions of different concentration of Biomolecules (in platinum electrode; scan rate, 100 mV $s^{-1,}$ concentration of NFX - 2×10^{-4} M; Biomolecule concentration ($M\times10^{-6}$) – 0.2, 0.4,0.8, & 1.0).

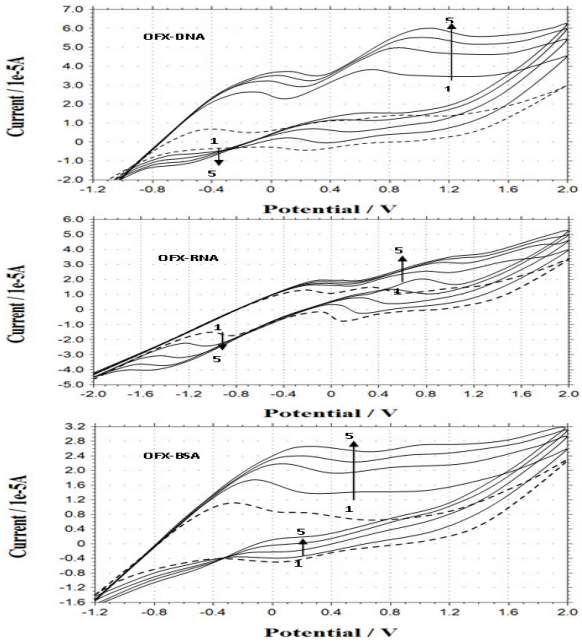

Figure - 7: Cyclic voltammograms of a platinum electrode in OFX with successive additions of a final concentration of Biomolecules with different scan rate = (100- 500 mV S^{-1}).

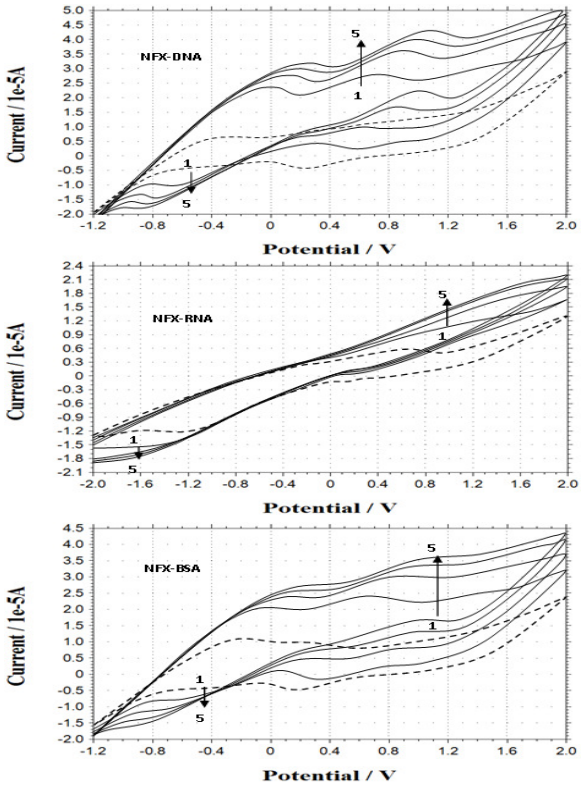

Figure – 8: Cyclic voltammograms of a platinum electrode in NFX with successive additions of a final concentration of Biomolecules with different scan rate = (100-500 mV S^{-1}).

In OFX, (i) the anodic and cathodic peak potential observed at -1183, 28, 1092 mv and -189 mv respectively, (ii) the anodic and cathodic peak

current observed at -4.01, -0.55, 2.62 mv and -1.62 mv respectively. **In NFX**, (i) the anodic and cathodic peak potential observed at -495, 179 mv and – 239, 320, 733 mv respectively, (ii) the anodic and cathodic peak current observed at -5.41, -6.01 mv and 11.1, 10.1, 11.3 mv respectively.

In OFX, upon increasing the concentrations of the biomolecules, (i) in DNA, the negative anodic peak potentials and anodic current peaks are increased, (ii) the difference in peak potential (ΔE_P) and difference in current peak (ΔI_C) are increased, (iii) in RNA, the negative anodic peak potentials and anodic current peaks are decreased, (iv) in BSA, the anodic peak potentials are increased and the negative anodic current peaks are increased.

In NFX, when the concentrations of the biomolecules increased, (i) in DNA the negative anodic peak potentials and anodic peak current are decreased, (ii) the difference in peak potential (ΔE_P) are increased and difference in current peak (ΔI_C) are decreased, (iii) however in RNA and BSA, the negative anodic peak potentials and anodic peak current are increased.

According to these observations, it seems that the decrease of peak currents of drug after an addition of excess DNA is caused by the interaction of drug to the bulky, slowly diffusing DNA, which results in a considerable decrease in the apparent diffusion coefficient. For measurement of binding constant (Kb) and binding site size (s)

The decay in peak current (Ip) of the drug by the addition of increasing amount of biomolecules can be used for the determination of binding constant and binding site size, whereas the shift in peak potential can be used to ascertain the mode of interaction. The binding constant is quantified by the following equation (4) [39]:

$$\log (1/ [\text{biomolecule}]) = \log K + \log (I/ (I_0 - I) \quad (4)$$

Where K is the binding constant, I_0 and I are the peak currents of the drug in the absence and presence of biomolecule respectively. The binding constant, K is obtained from the intercept of the plot of log(1/ [biomolecule]) vs. log (I/ (I_0 - I)). The effect of the addition of biomolecule to the OFX/ NFX solution on the wave voltammetry is changed. The current drops on the addition of biomolecule owing to the binding of OFX and NFX. The peak potential shifted to a more positive value in the presence of DNA. The shift in peak potential is typical of the intercalation of drugs into the biomolecules. In the presence of nucleic acids, the current is mainly due to free species, as the diffusion rate of bound species is small. The cause for the decrease in the peak current was that the obvious diffusion coefficient and the obvious concentration of electroactive species decreased.

The voltammetric response of the compound changed as is evidenced by the sequential drop in peak current and gradual peak potential shift in positive direction. The shift of peak potential to less negative values is suggestive of interaction of OFX/NFX into the biomolecules. The large peak to peak potential difference (ΔE_p) of -497 mV for OFX and -128 mV for NFX is suggest the electrochemical reaction coupled with a chemical reaction. From the cyclic voltammetry, it can be seen that the electrode reaction of OFX, NFX is a quasi-reversible process**.** The results indicate that the reaction is a diffusion-controlled process. When DNA, RNA and BSA was added to the OFX and NFX solution, both the oxidation and reduction currents increased [Figures 7, 8] indicating that an electrochemically non-active complex could have been formed. The formation of the complex resulted in the decrease of the equilibrium concentration of OFX and NFX in solution, leading to the increase of the peak current. DNA can provide three distinctive binding sites for the quinolone complexes; namely, groove binding, binding to phosphate groups, and intercalation. This behavior is of great importance with regard to the biological role of fluoroquinolone antibiotics in the human body [25]. The electrochemical reaction is more valuable to quantify the interaction parameters of an electro active molecule with DNA than other methods. By addition of different amounts of DNA to the voltammetric cell containing 1.0×10−6 M of drug, the cathodic peak currents of drug begin to decrease, and the formal potential shifts to more positive values which suggest the interaction of the drug with DNA.

Scan rate studies were carried out to investigate whether the process at the GCE was under diffusion or adsorption control. The effects of the potential scan rate between 100 and 500 mVs−1 on the peak current and potential of all complexes were evaluated. When the scan rate was varied from 100 to 500 mVs−1 in 1 × 10−6 mol L−1 complex solutions, a linear dependence of the peak current *I*p (μA) upon the square root of the scan rate $v1/2$ (mVs−1) was found by GCE demonstrating diffusional behavior. The effect of scan rate on peak current was also examined under the above conditions with a plot of logarithm of peak current versus logarithm of scan rate giving a straight line within the same scan rate range. These linear relationships were obtained as followed (n = 10 in all studies). In order to study the association constant (K_a)

between OFX and NFX with DNA, RNA and BSA, the cyclic voltammetry of the drugs with DNA, RNA and BSA were recorded at a scan rate of 100-500 mV s^{-1} [Figures 7, 8]. During the experimental process, the OFX and NFX concentration was kept constant and the concentrations of OFX, NFX were varied from $2.0x10^{-3}$ to $2.0x10^{-4}$ M.

Stoichiomerty of Drug-Biomolecule system was determined using voltammetric data. It was assumed that drugs interacted with biomolecules and formed complex. The binding number (m) and equilibrium constant (β) of the binding reaction can be deduced as follows:

$$\log[\Delta I/ (\Delta I_{max}-\Delta I)] = \log \beta + m \log[DNA] \quad (5)$$

The plot of E_p vs scan rate was linear shown in [Figure 9]. The plot of E_p vs ln v is well-defined straight line and the value can be calculated from the slope and ks from the intercept. The E^0 values of drugs can be determined from [Figure 10] on the ordinate by extrapolating the line to v = 0. The plot of log [ΔI/ (ΔImax – ΔI)] versus log[OFX] showed linearity with a correlation coefficient of 0.9992 [Figure 11]. The values of m and β were obtained from the slope and intercept of the plot. The value of m equal to unity indicated that a stable 1:1 complex is formed.

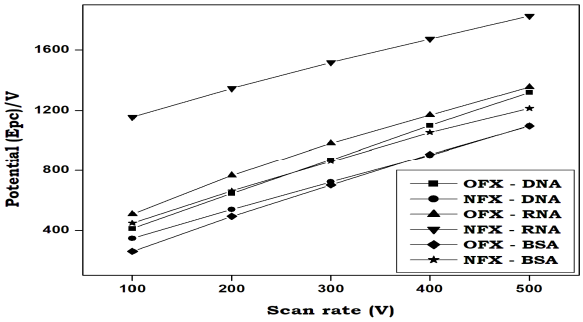

Figure - 9: Dependence of the peak potential E_p on the potential scan rate (ν) of drugs with DNA, RNA and BSA. [Scan rate - (100 to 500 m V S^{-1})].

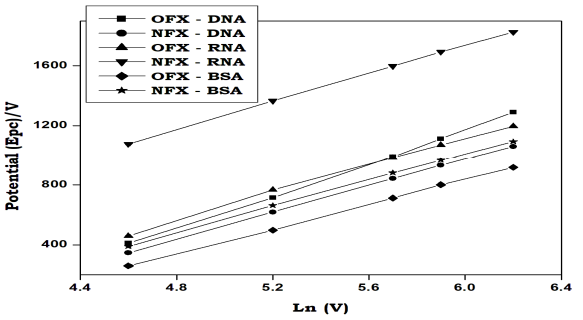

Figure - 10: Semilogarithmic dependence of the peak potential E_p on the potential scan rate (ln ν) of drugs with DNA, RNA and BSA. [Scan rate - (100 to 500 m V S^{-1})].

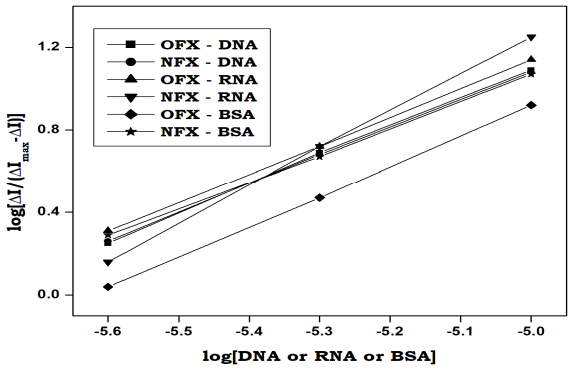

Figure - 11: Linear plot of log [Biomolecules] vs log [ΔI/ (ΔI_{max}- ΔI)]. Q- [DNA] (or) [RNA] (or) [BSA].

3.4. Molecular docking study

Molecular docking is a widely-used computational tool for the study of molecular recognition, which aims at predicting the binding mode in a complex formed by two or more constituent molecules with known structures. An important type of molecular docking is protein–drug docking because of its therapeutic applications in modern structure-based drug design. The computer simulated automated docking studies were performed using the widely distributed molecular docking software autodock 4.2.6. Among the various conformers of docking results, only 10 conformers were taken on the basis of the free energy of binding and score ranking. The minimum binding energy conformer is shown in [Figures 12-15] and all the data related to complexation and binding processes are reported in [Tables 6, 7]. We considered the binding free energy of the best ranked conformations as the main parameter for analysis of autodock 4.2.6 result. The autodock study of OFX and NFX was carried out and they were docked with in the biomolecules as shown in [Table 5] their autodock binding free energies (ΔG_b kcal/mol) and inhibition constants (K_i) were obtained. Among them all the drug exhibited the lowest free energy between -7.32 and -4.9 kcal/mol. In other words, they possess the highest potential binding affinity into the binding site of the 3D macromolecule. The computationally designed NFX showed less binding affinity than that of OFX. The higher affinity is presumably attributed to the formation of more and/or tighter hydrogen bonds between the several amino acids at the binding site owing to the increased electronegativity of the hydrogen and oxygen. Therefore OFX were docked deeply within the groove of the biomolecules and forming more hydrogen bonds with DG14, DG2, DG24, DG10 for dna and A32, A34, A31, U17, U16, for rna. and LYS533, GLN416, THR419, LYS533, LYS439, LYS20for bsa. further NFX was docked deeply

within the groove of the biomolecules and forming more hydrogen bonds with DA17, DG14. DG4, DG24, DA17, DG12, DC21 for DNA and U5, C46, C35, G10, U36, U17, A33, U4, A46, A34, U15 for RNA and LYS499, LYS533, TYR496, HIS3, ARG10, GLU293, LYS275, ASP172, GLU45, LYS64, ILE297 for BSA.

Considering the fitting of the NFX binding it was demonstrated that their binding energies were higher in comparison with the OFX. It is noteworthy that the NFX exhibited especially stronger binding affinities to possess the lower binding free energy -7.32 kcal/ mol and also OFX showed the binding free energy between -6.3kcal/mol. It was clarified that the derivatives possessing less binding free energy (-7.32 kcal/mol) are allowed to fit well into the groove of the binding site. The overall good correlation between the growth inhibitory activities of the NFX and the binding affinities predicted by auto dock was made clear as indicated in [Table 5]. A good docking interaction implies the prediction of drugs confirmation and orientation within targeted binding site and their lower interactions energies [40]. This efficacy and suitability of drugs was determined on the basis of binding energy calculations.

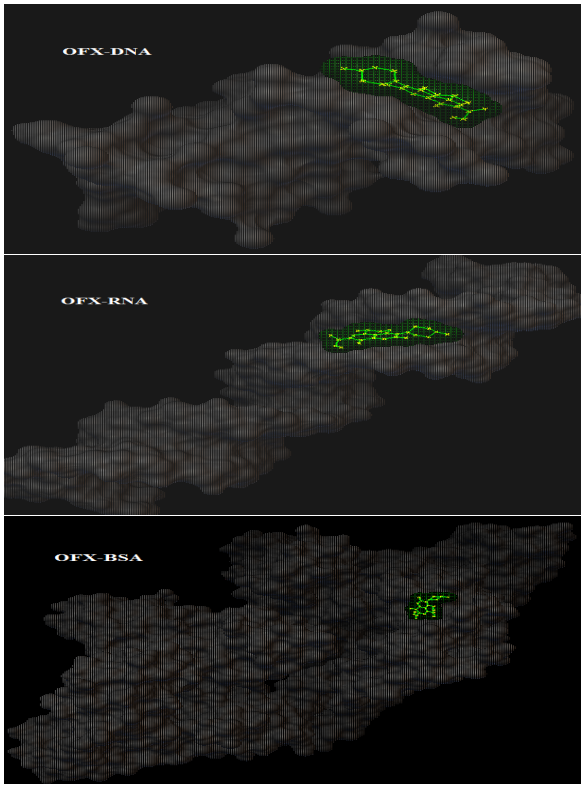

Figure – 12: Results of the GRID analysis searching for regions favorable for interaction of different OFX with Biomolecules. The protein is showed in white surface format and the drugs are showed in green "ball and stick" format.

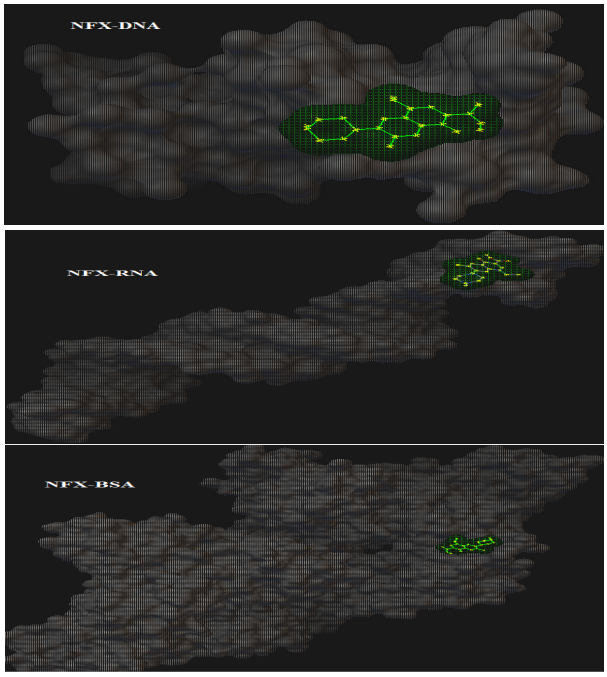

Figure - 13: Best binding mode between different NFX with Biomolecules. The protein is showed in backbone format and the drugs is showed in "ball and stick" format.

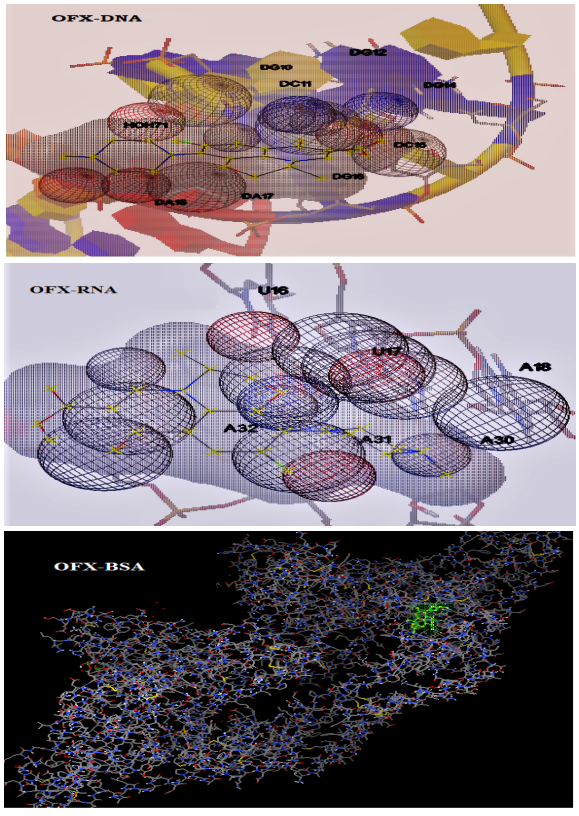

Figure – 14: Results of the GRID analysis searching for regions favorable for interaction of different OFX with Biomolecules. The protein is showed in white surface format and the drugs are showed in green "ball and stick" format.

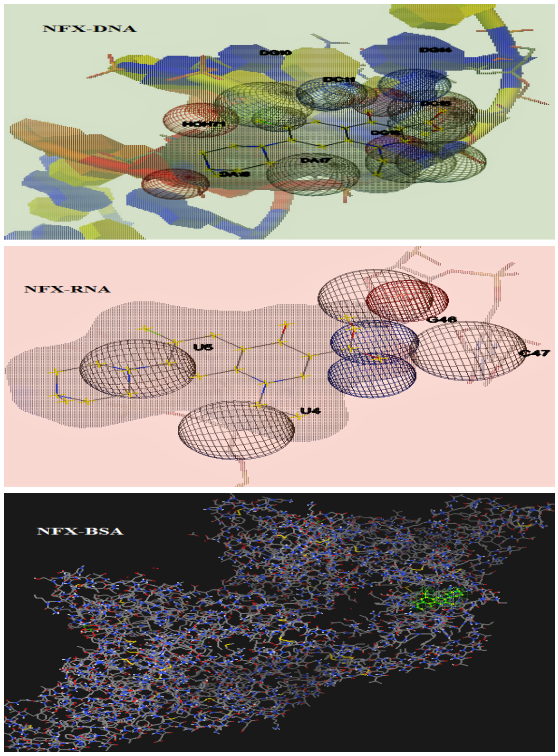

Figure - 15: Best binding mode between different NFX with Biomolecules. The protein is showed in backbone format and the drugs is showed in "ball and stick" format.

4. CONCLUSIONS

The present study particulates a spectroscopic, electrochemical and molecular docking investigation on the binding interaction of the potent antibacterial chemotherapeutic drug with the transport biomolecule. The study of the interactions with DNA has been performed with UV, Fluorescence spectroscopy, revealing that the drug bind to DNA. Drug exhibits much higher intrinsic binding constant to Drug-biomolecule. The results revealed the presence of a single binding site on DNA and its binding constants, K, are −7.78, −8.12 , −7.40 and -8.66, -7.89, 8.05 kcal mol^{-1}. The following results support that the drug can bind to DNA via two non intercalation modes. Thermodynamic studies indicate that the binding action of the drug and DNA is an exothermal reaction. However, a negative free energy change indicates that significant immobilization of drug and biomolecules occurs via hydrogen binding. In the subsequent interacting complex, the negative contribution to the overall ΔG may be associated with electrostatic interactions.In voltammetric studies, in the presence of DNA, the cyclic voltammograms of the drug exhibited a small negative shift in cathodic peak potentials followed by decrease in peak current, indicating the interaction existing between the drug and DNA Cyclic voltammetric studies show that all drug bind to DNA by both intercalation and electrostatic interaction.The docking method provided a means to estimate the participation and interactions of specific chemical groups in the process of complex stabilization at the molecular level. From the computational study, we find that negative complexation energy, Gibbs energy for the drugs indicate that the formation of these complexes is spontaneous and exothermic and hydrogen bonding interactions play a major role in the sensing process.

5. REFERENCE

1. Mahtab R, Rogers JP, Singleton CP and Murphy CJ. Preferential adsorption of a kinked DNA to a neutral curved surface. **J Amer Chem Soc**. 1996; 118: 7028–7032.
2. Erie DA, Yang G, Schultz HC and Busta-mante C. DNA bending by cro protein and nonspecific complexes: implications for protein site recognition and specificity. **Science.** 1994; 266: 1562–1566.
3. Ecker DJ and Griffey RH. **Drug Discov Today.** 1999; 4: 420.
4. Sucheck SJ and Wong CH. **Curr Opin Chem Biol**. 2000; 4: 678.
5. Peters TJ. Serum albumin. **Adv Protein Chem.** 1985; 37: 161–245.
6. Brown JR, Rosenoer VM, Oratz M and Rothschild MA. Albumin structure, function and uses. **Pergamon Oxford.** 1977; 27–51.
7. Peters TJ. All about albumin. **Academic San Diego**.1996.
8. He XM and Carter DC. Atomic structure and chemistry of human serum albumin**. Nature.** 1992; 358: 209–215.
9. Helms MK, Paterson CE, Bhagavan NV and Jameson DM. Time-resolved fluorescent studies on site-directed mutants of human serum albumin. **FEBS Lett**. 1997; 408: 67–70.
10. Sun C, Yang J, Wu X, Huang X, Wang F and Liu S. Unfolding and refolding of Bovine Serum Albumin induced by cetylpyridinium bromide. **Biophys J.** 2005; 88: 3518–3524.
11. Vasilescu M, Angelescu D, Almgren M and Valstar A. Interactions of globular proteins with surfactants studied with fluorescence probe methods. **Langmuir.** 1999; 15: 2635–2643.
12. Valstar A, Almgren M, Brown W and Vasilescu M. The interaction of Bovine Serum Albumin with surfactants studied by light scattering. **Langmuir.** 2000; 16: 922–927.

13. Deep S and Ahluwalia JC. Interaction of Bovine Serum Albumin with anionic surfactants. **Phys Chem Chem Phys**. 2001; 3: 4583–4591.

14. Das R, Guha D, Mitra S, Kar S, Lahiri S and Mukherjee S. Intramolecular charge transfer as probing reaction: fluorescence monitoring of protein-surfactant interaction. **J Phys Chem A**. 1997; 101: 4042–4047.

15. Ruiz-Peñaa M, Oropesa-Nuñeza R, Ponsb T, Louroc SRW and Pérez- Gramatgesa A. Physico-chemical studies of molecular interactions between non-ionic surfactants and Bovine Serum Albumin. **Colloids Surf B Biointerfaces.** 2010; 75: 282–289.

16. Aleixandre V, Herrera G, Urios A and Blanco M. **Antimicrob Agents Chemother**. 1991; 35: 20.

17. Swanson B, Boppana V, Vlasses P, Rotmen H and Ferguson R. Norfloxacin disposition after sequentially increasing oral doses. **Antimicrob Agents Chemother**. 1983; 23: 284–288.

18. Jimenez MC, Miranda MA and Vaya I. Triplet Excited States as Chiral Reporters for the Binding of Drugs to Transport Proteins. **J of Amer Chem Soc.** 2005; 127: 10134-10135.

19. Huey R, Morris GM, Olson AJ and Goodsell DS. A semiempirical free energy force field with charge-based desolvation. **J of Comput Chem.** 2007; 28: 1145–1152.

20. Morris GM and Lim-Wilby M. Molecular docking. In: Kukol A (ed) Molecular modeling of proteins, Methods in molecular biology. **Humana Totowa.** 2008; 443: 365–382.

21. Halgren TA. Merck molecular force field. I. Basis, form, scope, parameterization, and performance of MMFF94. **Journal of Computational Chemistry**. 1998; 17[5,6]: 490-519.

22. Rajendiran N and Thulasidhasan J. Interaction of sulfanilamide and sulfamethoxazole with bovine serum albumin and adenine: Spectroscopic and molecular docking investigations. **Spectrochim Acta**. 2015; 144: 183-191.

23. Rajendiran N and Thulasidhasan J. Study of the binding of thiazolyazoresorcinol and thiazolyazocresol dyes with BSA and adenine by Spectral, Electrochemical and Molecular docking Methods. **Canad ChemTrans**. 2015; 3: 291-30.

24. Rajendiran N and Thulasidhasan J. Binding of sulfamerazine and sulfamethazine to bovine serum albumin and nitrogen purine base adenine: a comparative study. **Inter Lett of Chem Phy and Astron**. 2015; 59: 170-187.

25. Rajendiran N and Thulasidhasan J. Spectral, electrochemical and molecular docking methods to get an understanding of supramolecular chemistry of sulfa drugs to biomolecules. **J. Mole Liqs**. 2015; 212: 857-864.

26. Rajendiran N and Thulasidhasan J. Spectral, electrochemical and molecular docking studies on the interaction of dothiepin and doxepin with BSA and DNA base, **The J of Bio and Chem Lumi**. 2016; 1–10.

27. Rajendiran N and Thulasidhasan J. Effects of interaction between Non-steroidal Anti-Inflammatory drugs with BSA and DNA base: Spectral, Electrochemical and Molecular docking methods. **J Indian Chem Soc**. 2017; 94: 83-93.

28. Benesi HA and Hildebrand JH. A spectrophotometric investigation of the interaction of iodine with aromatic hydrocarbons. **J Am Chem Soc**. 1949; 71: 2703–2707.

29. Park HR, Oh CH, Lee HC, Choi JG, Jung BI and Bark KM. **Bull Korean Chem Soc**. 2006; 27: 2002.

30. Xin Q, Zhong-Ying M, Cheng-Zhi X, Fei X. Yan-Wen Z, Jing-Yuan X, Zhao-Yan Q, Jian-Shi L, Gong-Jun C and Shi-Ping Y J. **Inorg. Biochem**. 2011; 105: 728.

31. Wang J. **Anal. Chim. Acta.** 2009; 469: 239.

32. Kelly TM, Tossi AB, McConnel DJ and Strekas TC. **Nucleic Acid Res**. 1985; 13: 6017.

33. Stephanos JJ. Drug-Protein Interactions: Two-Site Binding of Heterocyclic Ligands to a Monomeric Hemoglobin. **Journal of Inorganic Biochemistr**. 1996; 62: 155–169.

34. Marty R, Nsoukpoe-Kossi NC, Charbonneau D, Weinert CM, Kreplak L and Tajmir-Riahi HA. Structural analysis of DNA complexation with cationic lipids, **Nucleic Acids Res**. 2009; 37: 849–857.

35. Mallick A, Haldar B and Chattopadhyay N. Spectroscopic Investigation on the Interaction of ICT Probe 3-Acetyl-4-oxo-6,7-dihydro-12H Indolo-[2,3-a] Quinolizine with Serum Albumins. **The J of Phys Chem B**. 2005; 109: 14683-14690.

36. Barik A, Priyadarsini KI and Mohan H. Photophysical Studies on Binding of Curcumin to Bovine Serum Albumin. **Photochem and Photobio**. 2003; 77[6]: 597-603.

37. Kano K, Tawiya Y and Hashimoto S. Binding Forces in Complexation of p-Alkylphenols with β-Cyclodextrin and Methylated β-Cyclodextrins. **J. Incl. Phenom**. 1992; 3: 287.

38. Li DJ, Zhu JF, Jin J and Yao X.J. Studies on the binding of nevadensin to human serum albumin by molecular spectroscopy and modeling. **J. Mol. Struct**. 2007; 846: 34-41.

39. Feng Q, Li NQ and Jiang YY. Electrochemical studies of porphyrin interacting with DNA and determination of DNA. **Analytica Chimica Acta.** 1997; 344: 97–104.

40. Camacho CJ and Vajda S. Protein docking along smooth association pathways. **PNAS**. 2011; 98[19]: 1036–1041.